Modeling the Elastic Modulus of 2D Woven CVI SiC Composites

Gregory N. Morscher[1], Ohio Aerospace Institute, Brookpark, OH

ABSTRACT

The use of fiber, interphase, CVI SiC minicomposites as structural elements for 2D-woven SiC fiber reinforced chemically vapor infiltrated (CVI) SiC matrix composites is demonstrated to be a viable approach to model the elastic modulus of these composite systems when tensile loaded in an orthogonal direction. The 0^o (loading direction) and 90^o (perpendicular to loading direction) oriented minicomposites as well as the open porosity and excess SiC associated with CVI SiC composites were all modeled as parallel elements using simple Rule of Mixtures techniques. Excellent agreement for a variety of 2D woven Hi-Nicalon^{TM} fiber-reinforced and Sylramic-iBN reinforced CVI SiC matrix composites that differed in numbers of plies, constituent content, thickness, density, and number of woven tows in either direction (i.e, balanced weaves versus unbalanced weaves) was achieved. It was found that elastic modulus was not only dependent on constituent content, but also the degree to which 90^o minicomposites carried load. This depended on the degree of interaction between 90^o and 0^o minicomposites which was quantified to some extent by composite density. The relationships developed here for elastic modulus only necessitated the knowledge of the fractional contents of fiber, interphase and CVI SiC as well as the tow size and shape. It was concluded that such relationships are fairly robust for orthogonally loaded 2D woven CVI SiC composite system and can be implemented by ceramic matrix composite component modelers and designers for modeling the local stiffness in simple or complex parts fabricated with variable constituent contents.

INTRODUCTION

Woven silicon carbide fiber reinforced silicon carbide matrix composites with matrices fabricated by the chemical vapor infiltration route represent a very important

[1] Senior research scientist residing at NASA Glenn Research Center, Cleveland, OH

class of materials for a variety of high temperature air-breathing, space, and nuclear applications [1]. Future SiC/SiC components will possess rather complex shapes requiring various architectures, differences in local thickness, and local curvature, which may also lead to processing non-uniformities throughout a given component. Needless to say, in order to design with such materials, the effect of geometry, fiber-orientation, architecture, and constituent properties and content on stress-strain response needs to be well understood. The first and the foremost property required for component design is the effect of these factors on tensile elastic modulus. A significant amount of work has been performed towards understanding the mechanical properties of 2D [2-8] and 3D [5] woven CVI SiC matrix composites primarily with regard to the occurrence of non-linear stress-strain behavior due to matrix cracking. However, little has been done to quantify the elastic properties of these composites as a function of architecture, constituent properties, and constituent content. Therefore, the objective of this study was to determine relationships for the elastic modulus of 0/90 2D woven CVI SiC composites in the orthogonal directions for a wide variety of composite parameters by carefully accounting for all those parameters. The parameters included *architectural variations*, which included composite thickness, number of plies, balanced and unbalanced weaves, and tow size, and *constituent variations*, which included fiber-type, interphase composition, and constituent contents. In a companion paper [9], the effects of these same architectural and compositional parameters on matrix cracking were studied.

EXPERIMENTAL

Composite specimens with different CVI SiC matrix content were obtained from several processing approaches/anomalies representing vintages that span over 10 years from the same vendor (currently General Electric Power Systems Composite, Newark, DE). The three general processing approaches are shown schematically in Figure 1 and indicated in Table I. “Standard specimens” went through typical CVI fabrication and machining at General Electric Power Systems Composites, Newark, DE (Figure 1a). This consisted of woven fiber lay-up, CVI interphase infiltration, initial CVI SiC infiltration, specimen machining and a final CVI SiC infiltration step to further densify the specimen. Specimens consisting of eight to 36 plies were fabricated in this manner. Some

specimens, consisting of eight plies, were infiltrated to less than "full" matrix content (~ 50%) and not subjected to final CVI SiC infiltration. The open porosity in these low density matrices was filled with epoxy [10] (Figure 1b) for subsequent mechanical testing. In other studies, this fiber-interphase-CVI SiC "preform" makes up the skeleton of higher density composites where the open porosities are filled by SiC slurry and melt-infiltrated silicon composites [11]. However, for the purpose of this study they represent a very low CVI SiC content composite since the epoxy carries negligible mechanical loads. The third set of specimens were "thin panels" that consisted of one, two, or three plies that had delaminated from a multilayer woven SiC fiber, carbon fiber preform during CVI SiC infiltration [12] (Figure 1c). Even though these specimens were the product of delamination, the delamination occurred early in processing, so that cracking of CVI the SiC matrix was not observed in polished as-produced specimens.

As indicated in Table I, constituent variations included the woven fiber-type and interphase composition. Composites were fabricated with Hi-Nicalon^{TM} (HN) fibers (Nippon Carbon, Japan) woven at 6.7 tow ends per cm as a balanced five-harness satin or eight-harness satin weave or Sylramic-iBN fibers (Dow Corning, Midland, MI with a special NASA treatment [13]) woven into balanced (7.9 epcm) or unbalanced (9.4 epcm x 5.5 epcm) five-harness satin pieces of cloth. Fiber-preforms were either infiltrated with C or BN as the interphase. Specimens were machined as dog-bone specimens or straight-sided specimens, Table I identifies the specimen geometry of each specimen.

The constituent content was determined for each individual specimen from the mass of the specimens and relative weight gain information obtained from the composite manufacturer. This was necessary because CVI SiC content varies across a panel and some of the specimens were further densified after specimen machining. First, the mass of the as-processed and as-cut specimen was determined[*]. The dimensions were measured for each specimen shape to determine the specimen volume. The density was

[*] The mass for each specimen was determined in the as-machined ready-to-test state with the exception of the epoxy-infiltrated specimens. The epoxy-infiltrated specimens were weighed after the perform panel was cut into straight-sided specimens and prior to epoxy-infiltration and dogbone machining for constituent determination. The weight of the after-epoxy specimen was measured as well.

determined for each specimen from the mass and specimen volume. The average total fiber volume fraction was determined from the fiber tow and weave properties as follows:

$$f_f = \frac{N_{ply} N_f \pi R_f^2 \left(epmm_0 + epmm_{90} \right)}{t} \qquad (1)$$

where N_{ply} is the number of woven plies, N_f is the number of fibers per tow (500 for Hi-Nicalon and 800 for Sylramic-iBN), R_f is the average fiber radius (0.00685 μm for Hi-Nicalon and 0.005 μm for Syl-iBN as measured from polished cross-sections of several composites), t is the average specimen thickness, and *epmm* is the number of tow ends per mm, and subscripts *0* and *90* refer to the orthogonal directions

The fraction of the interphase material, f_i, was determined as follows:

$$f_i = \frac{f_f m_i \rho_f}{m_f \rho_i} \qquad (2)$$

where m_f is the mass of the fiber preform before tooling, m_i is the mass of the interphase by subtracting the mass of the interphase coated preform from the fiber-only preform mass, and ρ_f and ρ_i are the densities of the fiber (2.71 g/cc for Hi-Nicalon and 3.05 g/cc for Sylramic-iBN) and interphase, respectively. The density of the interphase was assumed to be 1.5 g/cc for BN [14] and C. This value may be in error; however, f_i is relatively insensitive to the analysis below. The CVI SiC volume was then determined as follows:

$$V_{SiC} = \frac{V_{spec}}{\rho_{SiC}} \left(\rho_{spec} - \rho_f f_f - \rho_i f_i \right) \qquad (3)$$

where V_{spec} is the specimen volume, ρ_{spec} is the specimen density, and ρ_{SiC} is the density of CVI SiC (3.2 g/cc). The volume fraction of SiC matrix, f_{SiC}, is then simply V_{SiC}/V_{spec}. Finally, the average total fraction of porosity for each specimen could be estimated from the constituent volume fractions:

$$f_p = 1 - f_f - f_i - f_{SiC} \quad (4)$$

The constituent fractions are listed in Table I.

Room temperature tensile testing was performed using a universal-testing machine (Instron 8562, Instron Ltd., Canton, Mass.) and strain was measured with a clip-on extensometer (2.5% maximum strain range over a 25.4 mm gage length). For some of the tensile tests, three wide-band acoustic emission (AE) sensors were attached to the specimen, which is described in the companion paper [9]. Specimens were either tested monotonically to failure or were loaded, unloaded, and reloaded at a higher load until failure occurred. The loading rate was 2 kN/min for the thin specimens, 4 kN/min for standard specimens, and 10 kN/min for the thick specimens.

RESULTS

The composites differ considerably in numbers of plies (1 to 36), thickness (0.38 to 10.6 mm), and constituent content (Table I). Most notably, f_{SiC} varied by nearly a factor of two and f_p varied by nearly a factor of three for the Hi-Nicalon composites. There was also significant variation in f_f and some composites fabricated with a carbon interphase for each fiber-type had significantly higher interphase content than the other specimens (Table I).

Microstructure

Some of the composite microstructures are shown in Figure 2 for HN composites (a-g) and SYL-iBN composites (f-i). Longitudinal sections refer to sections cut and polished along the length of the tensile specimen, whereas the cross section (Figure 2c) refers to the section cut perpendicular to the length of the tensile specimen. The microstructure differs considerably. For the thick specimens (Figure 2d), the exterior plies have a high CVI SiC content whereas the inner plies have larger unfilled regions, typical of preferential SiC deposition. For the epoxy-infiltrated high-porosity specimens (Figure 2e), the structure is very open. Note how nearly all the coated tows are separate from one another. Noted in Figure 2a is the 0^o minicomposite, i.e., the region of fiber, interphase, and CVI SiC matrix oriented in the loading direction, and the 90^o

minicomposite, i.e., the region of fiber, interphase, and CVI SiC matrix oriented perpendicular to the loading direction. This will become important later in the analysis. Also, the effect of fiber-type results in different tow sizes which is a product of the weave, compaction of the ply lay-up by the manufacturer, total fiber count and fiber diameter. The cross-sectional area of fibers in a Hi-Nicalon tow is about 22.5% greater than the Sylramic-iBN tow. Note also that some axially-oriented porosity exists within the tows.

Stress-Strain Behavior and Ultimate Failure

Room-temperature stress-strain curves obtained by tensile loading along the fiber orthogonal directions are shown in Figure 3 for the different composite systems. As expected, the composites with the lowest porosities had relatively high elastic moduli, whereas the specimens with the highest porosities (epoxy-infiltrated and thin panels) had lower elastic moduli. There was also much variation in non-linear stress-strain behavior and ultimate tensile strength which will be discussed and analyzed in the companion paper [9].

Elastic Modulus and Speed of Sound of Undamaged Composites

The effect of constituent content on elastic modulus was analyzed for a variety of constituents and physical parameters. On an empirical basis, composite modulus proved to exhibit the best correlation with composite density (Figure 4). There appears to be two regions, a region of higher density where there is a strong relationship between density and E and a lower density region where there is a mild relationship between density and E.

The speed of sound of each specimen was used as a check to the measurements of E and ρ. Sound waves were created by pencil lead-breaks or by the matrix microfractures that occur near or in the grips at very low loads [9]. The speed of sound could be determined from the difference in time of arrival of the first peak of the relatively non-dispersive extensional wave [15]. Figure 5 shows a plot of speed of sound versus $(E/\rho)^{1/2}$ for a number of monolithic materials and the composites tested in this study. Note that under plane strain behavior, it would be proper to compare the measured elastic

moduli with $(E/[\rho(1-\nu^2)])^{1/2}$, where ν is Poisson's ratio. However, ν was not known for the composites and was assumed to have a minor affect on the analysis since ν would be ~ 0.2 ± 0.1. The speeds of sound of the monoliths fall just below a line of direct proportion, due to the absence of ν in the comparison. The speeds of sound of the composites fall near the same line indicating a good correlation of measured elastic modulus and density.

Modeling Elastic Modulus: The Role of the 90° Minicomposite

Similar to reference 6, the entire composite can be considered to consist of 0° (stressed direction) and 90° (perpendicular to stress direction) oriented fiber-interphase-CVI SiC minicomposites. In this construction, the minicomposite is not necessarily a uniform mixture, unlike 0/90 laminate composites [16-17], but may contain two distinct regions: an inner region consisting of a mixture of fibers, interphase coating, CVI SiC and inner-tow porosity surrounded by an outer "shell" of CVI SiC if a sufficient amount of SiC is infiltrated to fill the inner region (Figure 6a and b). In addition, there are typically large open pores associated with weave crossover points and depends on the degree of "nesting" achieved after ply stacking and pressing.

The difficulty in modeling the elastic modulus of woven composites comes with the treatment of the 90° minicomposites and the network of open porosity. The large open porosity in composites is sometimes associated with 0° minicomposites and can be considered in parallel to the loading direction; however, some large pores are associated with the 90° minicomposites and would appear to be in series in a given ply. The large pores associated with the 90° plies would increase as *epcm* decreases for the 90° orientation. On the other hand, nesting, ply compaction, and the registry of ply lay-up can minimize the porosity within and between plies. Also, if the porosity is on average well-distributed in a cross-section and good transfer of load exists between 0° and 90° minicomposites over a critical length scale in the loading direction, it is possible that all of the open porosity can be treated in parallel. The approach here will be to determine in general the degree of load carried by the 90° minicomposites assuming that all of the large open porosity acts in parallel under load. Then a model for the elastic modulus of

the 90^o minicomposites will be developed based on constituent content in order to predict the composite elastic modulus for the different CVI SiC composites studied.

First it is assumed that all of the condensed phases in the composite are associated with 0^o and 90^o oriented tow minicomposites (Figure 6a). To determine the degree of load-carrying contribution for the 90^o minicomposites, it is first assumed that three elements, 0^o minicomposites, 90^o minicomposites, and open porosity, act in parallel and can therefore be described by the Rule of Mixtures:

$$A_c \varepsilon_c E_c = A_0 \varepsilon_0 E_0^* + A_{90} \varepsilon_{90} E_{90}^* + A_{open\text{-}por} \varepsilon_{open\text{-}por} E_{open\text{-}por} \qquad (5)$$

Where A is area, ε is strain, E^* is the elastic modulus of the 0^o and 90^o minicomposites and subscripts "c" and "open-por" refer to composite and open porosity, respectively. The total porosity (Table I) is the sum of the open porosity and the inner porosity (the porosity contained within the minicomposite estimated here to be ~ 5% of the composite volume). E_{90}^* and E_{90}^* are considered to be the effective moduli of the entire 0^o and 90^o minicomposites as depicted in Figure 6a. E_{90}^* then describes the load-carrying ability of the 90^o minicomposite.

Assuming equivalence of the strain terms and $E_{open\text{-}por} = 0$, the volume fraction of minicomposites is the area of the minicomposites divided by the area of the composite, and solving for E_c reduces Equation 5 to:

$$E_c = f_0 E_0^* + f_{90} E_{90}^* \qquad (6)$$

Where f_0 and f_{90} are the volume fractions of 0^o and 90^o oriented minicomposites and can be represented by:

$$f_0 = l_0 (f_f + f_i + f_{SiC} + f_{inner\text{-}por}) \qquad (7a)$$

$$f_{90} = (1 - l_0) (f_f + f_i + f_{SiC} + f_{inner\text{-}por}) \qquad (7b)$$

where $f_{inner\text{-}por}$ is the total fraction of porosity in the inner region of a minicomposite (~ 0.05) and l_0 is the ratio of fibers oriented in the loading direction:

$$l_0 = \frac{epcm_0}{epcm_0 + epcm_{90}} \tag{8a}$$

For a balanced weave, $l_0 = 0.5$.

E_0^* can simply be determined from Rule of Mixtures of the constituent content of the 0^o minicomposites:

$$E_0^* = \frac{l_0\left(f_f E_f + f_i E_i + f_{SiC} E_{SiC}\right)}{f_0} \tag{9}$$

Where E_f = 380 GPa for Sylramic-iBN and 280 GPa for Hi-Nicalon, E_{SiC} = 425 GPa for CVI SiC, and E_i = 23 GPa (see below). Then, E_{90}^* can be backed out from equation 6:

$$E_{90}^* = \frac{\left(E_c - f_0 E_0^*\right)}{f_{90}} \tag{10}$$

Figure 7 shows the relative load carrying ability of the 90^o minicomposites as plotted against density. There is a striking demarcation between high density and low density composites. The higher density composites exhibit significant load-sharing in the 90^o minicomposites whereas in the low density minicomposites, the 90^o minicomposites exhibit little or no actual contribution to load-sharing. Physically this implies that *a sufficient amount of CVI SiC is necessary to insure good interaction or strong bonding between adjacent plies so that the 90^o are loaded.* This explains why there was little effect of density on E_c for the low density composites (Figure 4). Practically then, for low density composites, it can be assumed that the 90^o minicomposites do not share the load:

$$E_c \text{ (low density)} = f_0 E_0^* \tag{11}$$

Modeling Elastic Modulus: High Density Composites

For higher density composites it is obvious that the 90° minicomposites carried significant load. The minicomposite consists of the two regions mentioned above: the inner region of the minicomposite and the outer region of CVI SiC (Figure 6). The inner region of the 90° minicomposite is the most difficult entity to model. One unknown quantity is the elastic modulus of the low-temperature deposited CVI BN. The composite specimens where there was very little porosity in between 90° minicomposites, the Syl-iBN composites oriented with the 5.5 epcm in the 0° direction (Figure 2h), was used to "back out" the elastic modulus of the inner region of the 90° minicomposite and to estimate E_i. For this case, nearly all of the porosity is aligned axially (Figure 2g would correspond to a cross-section where the 5.5 epcm orientated tows are loaded). Also, nearly all of the CVI SiC that is infiltrated outside of the inner region of the minicomposites is well situated with the 0° tows or the surface of the composite enabling good load transfer to this portion of CVI SiC and would fulfill the requirement that the CVI SiC outside of the inner region of the minicomposite operates in parallel. Therefore, the "outer SiC" corresponding to 0° minicomposites, 90° minicomposites, and the surface of the composites will be treated as one entity and the "inner region" of the minicomposites will be modeled separately. Since the inner region of the 0° minicomposites, the outer-SiC, and the open porosity were all aligned in parallel to the loading direction, the elastic modulus of the inner region of the 90° minicomposites could be determined from rule of mixtures:

$$E_{inner90} = \frac{E_c - f_{inner0}E_{inner0} - f_{outerSiC}E_{SiC}}{f_{inner90}} \qquad (12)$$

where "inner" refers to the inner region of a minicomposite. The fractions of the inner regions of the minicomposite are simply:

$$f_{inner0} = f^0_{f-inner} + f^0_{i-inner} + f^0_{SiC-inner} + f^0_{porosity-inner} \qquad (13a)$$

$$f_{inner90} = f^{90}_{f-inner} + f^{90}_{i-inner} + f^{90}_{SiC-inner} + f^{90}_{porosity-inner} \qquad (13b)$$

For a balanced composite, with the same tow size in the orthogonal directions, f_{inner0} and $f_{inner90}$ would be equivalent. Since all of the fibers and the interphase coating are contained in the inner regions of the minicomposite:

$$f_{j-inner}^{0} = l_0 f_j \tag{14a}$$

$$f_{j-inner}^{90} = (1 - l_0) f_j \tag{14b}$$

where subscript *j* pertains to *f*, *i*, and *porosity-inner*. $f_{SiC\text{-}inner}$ can only be determined if f_{inner} is known. This depends on the volume (area) of the tow, which may differ for different architectures. The two dimensions, height (2a) and width (2b), of the inner regions of the tows (Figure 6b) were measured for representative specimens from each panel for both orthogonal directions (Table II). There was essentially no difference in tow size of the orthogonal minicomposites for a given balanced panel. There was very little difference in tow dimensions for different panels with balanced architectures and the same fiber types. There were also minor differences measured for the two orthogonal directions in the unbalanced composites. The actual shape of a cross-section of a tow varies between an ellipse and a rectangle. The latter was chosen here to describe the tow cross-section:

$$f_{inner}^{0} = \frac{A_{inner}^{0}}{A_{tot}} = \frac{epmm_0 \, 2a_0 \, 2b_0 N_{ply}}{t} \tag{15a}$$

$$f_{inner}^{90} = \frac{A_{inner}^{90}}{A_{tot}} = \frac{epmm_{90} \, 2a_{90} \, 2b_{90} N_{ply}}{t} \tag{15b}$$

where A_{tot} is the cross-sectional area of the composite. $f_{SiC\text{-}inner}$ can then be determined from Equations 13a and b for the 0^o and 90^o orientations, respectively. $E^o_{innerSiC}$ can be determined from the rule of mixtures and the fraction of outer-SiC as follows:

$$f_{outerSiC} = f_{SiC} + f_{SiC-inner}^{0} + f_{SiC-inner}^{90} \tag{16}$$

Equation 12 was solved for the Sylramic-iBN composite specimens where the 5.5 epcm tows were aligned in the loading direction. $E_{inner90}$ was found to be 140 $\pm$ 5 GPa for two specimens.

Next, the inner 90^o elastic modulus can be modeled for the unbalanced Syl-iBN composite oriented with the 5.5 epcm tows in the loading direction. In reference 6, it was assumed that the fibers in the 90^o minicomposite act as pores due to poor load transfer through the weak interface. For the composites of this study, it is evident that the 90^o minicomposites do carry significant loads (Figure 7). If there is enough load transfer within the inner region of the 90^o minicomposite, the elastic modulus must be accounted

for. However, E_i of BN deposited at low temperatures is not well understood. In another study, it was assumed that the elastic modulus of the nanocrystalline randomly oriented BN was 62 GPa [14]. The elastic modulus of low temperature derived BN ranges from 10 to 200 GPa [18-20] depending on orientation and crystallinity. Since $E_{inner90}$ was estimated for the composites with the 5.5 epcm tows oriented in the loading direction, a simple Reuss element (Equation 17) was used to model E_{inn90} from which E_i could be backed out. The best fit E_i equaled 23 GPa. This value corresponds well with the elastic modulus of BN (20 GPa) in similar composites measured by nanoindentation [21].

$$E_{inner90} = \left(\frac{f_{inner-i}}{E_i} + \frac{f_{inner-f}}{E_f} + \frac{f_{innerSiC}}{E_{SiC}} \right)^{-1} \qquad (17)$$

Finally, the same approach and assumptions (0^o inner minicomposite, outer SiC, macroporosity, and 90^o inner minicomposite all act in parallel) were applied to model the elastic modulus of all the higher density composites. Two extremes were modeled for $E_{inner90}$. The high stiffness extreme used Equation 17 to estimate $E_{inner90}$ with E_i assumed to be 23 GPa. The low stiffness extreme assumed $E_{inner90} = 0$, i.e., poor load-transfer or fiber-matrix decoupling within the inner region of the minicomposite. The Rule of Mixtures relationship, Equation 12 (solved for E_c), was used to determine E_c. Figure 8 plots the measured E_c vs the predicted E_c for the Sylramic-iBN and Hi-Nicalon composite systems. For the lower density Hi-Nicalon composites, Equation 11 was used to predict E_c. Table III lists the measured and estimated moduli for each specimen.

There is excellent agreement between predicted and measured E_c for the Sylramic-iBN composites regardless of interphase or orientation when using the Reuss model to describe $E_{inner90}$. The Hi-Nicalon composites are in good agreement for the Reuss model; however, the predicted E_c tended to overestimate the measured value. The lower extreme prediction, $E_{inner90} = 0$, underestimated the measured E_c for all the higher density composites except for the 8 ply carbon interphase Hi-Nicalon CVI SiC.

DISCUSSION:

The elastic modulus of the CVI SiC matrix composites was predicted by applying simple Rule of Mixture techniques for a wide range of constituent content, ply lay up, fiber-type, woven fiber tows per length, balanced weave and unbalanced weave. The

good correlation between prediction and measured values appears to vindicate the simple assumptions that went into the analysis. This approach should also provide designers with simple, yet fairly robust, relationships for modeling the elastic modulus of 2D woven CVI SiC matrix composites in the orthogonal direction. The entire analysis requires only the knowledge of the fractional contents, f_f, f_i, and f_{SiC}, of the condensed phases and the general shape, balance, and size of the tows. This could easily be incorporated into modeling the local stiffness of a component if the local constituent contents and tow shape of a complex component are known from process models, microstructural evaluation, and/or NDE techniques where local processing variation may occur due to nonuniform infiltration of interphase or more likely CVI SiC. It should also be noted that the stiffness in off-axis directions measured by others [4] and determined by the speed of sound as a function of orientation [22] for panels of similar high density composites show only a slightly lower modulus (~ 5%) than the orthogonal directions. This is presumably due to the fact that this property is dominated by the CVI SiC. Therefore, once E is known in the orthogonal directions, a slight "knock down" modification can be made as a function of orientation.

The demarcation between low and high density that dictated the change in elastic modulus was not determined absolutely in this study. It was found that the stiffness of composites less than ~ 2.0 g/cc was controlled by the 0^o minicomposites whereas composites greater than ~ 2.3 g/cc had significant load-shared by the 90^o minicomposites. This result points to a lack of interaction between 90^o minicomposites with 0^o minicomposites at the lower densities probably due to low CVI SiC contents. It may also be due in part to large pores acting more in series rather than in parallel when loaded. It is not known whether there is a clear demarcation between these two regions or whether there will be a gradual transition from one to the other.

There was greater variability in the predicted elastic moduli for Hi-Nicalon composites. The largest overestimate of the predicted E_c for the high-density Hi-Nicalon composites was never greater than 11% of the measured E_c value. The reason for this is unknown. There were differences in interphase compositions; however, the interphase composition did not appear to affect predictability. The degree of bonding between Hi-Nicalon fibers and the interphase may be weaker than that for the Sylramic-iBN. The Hi-

Nicalon fiber has a smooth sometimes carbonaceous surface mating the interphase. This may lead to poorer bonding and load-sharing when loaded transversely. The Sylramic-iBN has a rough surface where the outer ~ 100 μm of the fiber was converted to a crystalline BN which would be expected to provide better bonding and load transfer. It should be noted that Sylramic-iBN composites fabricated with an already debonded interphase/matrix interface (outside debonding) had a significantly lower E_c when compared to composites of the same constituent content that did not show the same degree of processing-induced debonding [23].

It is evident that significant load is carried by the inner regions of the 90° minicomposites when good interaction between 90° and 0° is achieved with high enough CVI SiC contents. On average, $E_{inner90}$ for typical HN 90° minicomposites (excluding the HN 8PLY C interphase composite) was approximately 175 GPa and for typical Sylramic-iBN 90° minicomposites (excluding the 7.9 epcm Syl-iBN C interphase composite) was approximately 150 GPa. There was some minor variation from panel to panel due to minor differences in constituent fraction content (Table III). Note that for the thick interphase composites, HN 8PLY(C) and 7.9 epcm Syl-iBN (C) composite specimens, $E_{inner90}$ is significantly lower because very little CVI SiC actually penetrates the inner region of the minicomposite. For the HN 8PLY(C) composite, the low modulus for $E_{inner90}$ still resulted in an overestimate of the measured E_c. For that case, $E_{inner90} = 0$ was the best predictor. For the 7.9 epcm Syl-iBN (C), the low modulus for $E_{inner90}$ worked very well in predicting E_c.

Finally, with a model for E_c, the full linear and non-linear behavior of 2D woven CVI SiC composites can be modeled. It will be shown in the companion paper [9] that the matrix crack density for the high density composite can be simply modeled by the stress in the CVI SiC as determined by local elastic strain which necessitates E_c to be known for a given system. It is also believed that this approach serves as a basis for modeling E_c in dense melt-infiltrated composites by filling in most of the porosity with Si and SiC. This will be the focus of a future study.

CONCLUSION

The elastic modulus of woven SiC fiber-reinforced, CVI SiC matrix composites stressed in one of the orthogonal directions could effectively be modeled by assuming that the basic structural elements of the composites are the 0^o oriented (loading direction) and 90^o oriented fiber, interphase, and CVI SiC minicomposites. This was accomplished for a wide variation of constituent content, fiber-type, ply lay-up, and interphase content. The effect of constituent content on elastic modus not only depends on the relative amounts of constituents, but also on the effectiveness of the structure, i.e., 90^o minicomposites, to carry load. Lower density composites have very little load-carrying contribution from 90^o minicomposites when loaded in the 0^o direction whereas significant load was carried by the 90^o minicomposites for higher density composites. The treatment of the inner region of the 90^o minicomposite as a series element (Reuss model) of the three condensed phases proved to be most effective towards predicting the elastic modulus of the higher density composites. It is concluded that this represents a very simple yet robust approach to modeling the stiffness of 2D woven SiC fiber-reinforced SiC matrix composites when loaded in the orthogonal direction that can be implemented by designers rather easily.

REFERENCES

1. R. Naslain, "Design, preparation and properties of non-oxide CMCs for application in engines and nuclear reactors: an overview" *Comp. Sci. Tech.*, 64 (2004) 155-170.
2. Guillaumat, L. and Lamon, J., "Multi-fissuration de Composites SiC/SiC," in Revue des Composites et des Materiaux Avances, vol. 3, 1993, pp. 159-171.
3. Guillaumat, L. and Lamon, J., "Probabilistic-Statistical Simulation of the Non-Linear Mechanical Behavior of a Woven SiC/SiC Composite," *Composites Science and Technology*, Vol. 56, 1996, pp. 803-808.
4. X. Aubard, J. Lamon, and O. Allix, "Model of the Nonlinear Mechanical Behavior of 2D SiC-SiC Chemical Vapor Infiltration Composites," J. Am. Ceram. Soc., Vol. 77, No. 8, (1994) pp. 2118-26

5. Pluvinage, P., Parvizi-Majidi, A., and Chou, T.W., "Damage Characterization of Two-Dimensional woven and Three-Dimensional Braided SiC-SiC Composites," *Journal of Materials Science,* Vol. 31, 1996, 232-241.
6. J. Lamon, B. Thommeret, and C. Percevault, "Probabilistic-statistical Approach to Matrix Damage and Stress-Strain Behavior of 2-D Woven SiC/SiC Ceramic Matrix Composites," *J. European Ceramic Society*, 18 (1998) 1797-1808
7. J. Chevalier, M. Huger, D. Fargeot, and C. Gault, "Ultrasonic Investigation of the Time-dependent Damage in a 2D SiC/SiC Composite Under Static Loading," *J. European Ceramic Society*, **18** (1998) 1857-1867
8. J. Lamon, "A Micromechanics-based Approach to the Mechanical Behavior of Brittle-Matrix Composites," *Comp. Sci. Tech.*, 61 (2001) 2259-2272
9. G. Morscher, M. Singh, J. Kiser, R. Bhatt, and M. Freedman, "Stress-Dependent Matrix Cracking in CVI SiC Composites", submitted to Comp. Sci. Tech.
10. R.T. Bhatt, Y.L. Chen, and G.N. Morscher, "Microstructure and tensile properties of BN/SiC coated Hi-Nicalon, and Sylramic SiC fiber performs," J. Mater. Sci., Vol. 37, pp. 3991-3998 (2002)
11. D. Brewer, "HSR/EPM Combustor Materials Development Program", Mater. Sci. Eng. A, Vol. A261 (1999) pp. 284-291.
12. G.N. Morscher and M. Singh, Thermo-Mechanical Performance of Multilayer C and SiC Fiber-Reinforced, CVI SiC Matrix Composites", presented at 28th International Cocoa Beach Conference on Advanced Ceramics and Composites (2004)
13. H.M. Yun and J.A. DiCarlo, "Comparison of the Tensile, Creep, and Rupture Strength Properties of Stoichiometric SiC Fibers," Cer. Eng. Sci. Proc., 20 [3] 259-272 (1999)
14. S.K. Mital, M. Tong, P.L.N. Murthy, and J.A. DiCarlo, "Micromechanics-Based Modeling of Thermal and Mechanical Properties of an Advanced SiC/SiC Composite Material," NASA/TM – 97-206295 December, 1997
15. G.N. Morscher, Comp. Sci. Tech., "Stress-Dependent Matrix Cracking in 2D Woven SiC-fiber Reinforced Melt-Infiltrated SiC Matrix Composites," Vol. 59, No. 5 (1999) pp. 687-697

16. D.S. Beyerle, M. Spearing, and A.G. Evans, "Damage Mechanisms and the Mechanical Properties of a Laminated 0/90 Ceramic/Matrix Composite," J. Am. Ceram. Soc., 75 [12] 3321-30 (1992)
17. C. Xia, R.R. Carr, and J.W. Hutchinson, "Transverse Cracking in Fiber Reinforced Brittle Matrix Cross-Ply Laminates," Acta Metall. Mater., 41 [3] 2365-76 (1993)
18. J. Vilcarromero, M.N.P Carreno, I.Pereyra, "Mechanical properties of boron nitride thin films obtained by RF-PECVD at low temperatures," Thin Solid films 373 (2000) 273-276
19. J-G Kho, K-T Moon, J-H Kim, and D-P Kim, "Properties of Boron Nitride (BxNy) Films Produced by the Spin-Coating Process of Polyborazine," J. Am. Ceram. Soc., 83 [11] 2681-2683 (2000)
20. H.Vincent, F. Chassagneux, C. Vincent, B. Bonnetot, M.P. Berthet, A. Vuillermoz, and J. Bouix, "Microtexture and structure of boron nitride fibres by transmission electron microscopy, X-ray diffraction, photoelectron spectroscopy, and Raman scattering," Mater. Sci. Eng. A340 (2003) 181-192
21. G. Ojard and Y. Gowayed, presented at Advanced Ceramics and Composites Meeting, Cocoa Beach, FL, January 24th, 2005
22. G. N. Morscher, unpublished research.
23. G.N. Morscher, H.M. Yun, J.A. DiCarlo, and L. Thomas-Ogbuji, "Effect of a Boron Nitride that Debonds Between the Interphase and the Matrix in SiC/SiC Composites," *J. Am. Ceram. Soc.*, **87** [1] 104-12 (2004)

Table I: Physical Properties of Composite Specimens

Specimen (interphase) {no. specimens}	Weave	Specimen shape	t, mm	f_f	f_i	f_{SiC}	f_p
Hi-Nicalon Composites							
Standard 8 Ply Panels							
8 Ply (C) {2}	8HS	dog-A[a]	2.84	0.28	0.13	0.44	0.15
8 Ply (BN1) {2}	8HS	dog-A	2.37	0.37	0.05	0.41	0.17
8 Ply (BN2) {2}	5HS	dog-B[b]	2.53	0.31	0.06	0.48	0.15
8 Ply (BN3) {1}	5HS	dog-B	2.14	0.33	0.05	0.47	0.15
Standard Thick Panels							
30 Ply (C) {1}	5HS	dog-B	8.68	0.34	0.04	0.45	0.17
36 Ply (C) {1}	5HS	dog-B	10.56	0.34	0.04	0.43	0.19
Thin Panels							
1 Ply (C) {1}	5HS	Straight[s]	0.38	0.26	0.04	0.29	0.41
2 Ply (C) {2}	5HS	Straight	0.73	0.28	0.04	0.33	0.35
3 Ply (C) {2}	5HS	Straight	0.92	0.32	0.04	0.35	0.29
Epoxy Iniltrated Panels							
E8Ply-5HS(BN1) {1}	5HS	dog-B	2.45	0.32	0.05	0.25	0.38
E8Ply-5HS(BN2) {1}	5HS	dog-B	2.45	0.32	0.05	0.27	0.35
E8Ply-8HS(BN) {1}	8HS	dog-B	2.37	0.33	0.05	0.29	0.33
Sylramic-iBN Composites (Standard 8 Ply Panels)							
8 Ply 7.9 epcm (1) {1}	5HS	dog-A	2.18	0.363	0.071	0.377	0.189
8 Ply 7.9 epcm (2) {1}	5HS	dog-A	2.17	0.365	0.069	0.387	0.179
8 Ply 7.9 epcm (3) }1}	5HS	dog-A	2.19	0.361	0.070	0.443	0.126
8 Ply 7.9 epcm (C) {1}	5HS	dog-A	2.38	0.332	0.229	0.346	0.093
8 Ply Unbalanced {4}	5HS	dog-A	2.24	0.335	0.069	0.464	0.132

[a] Dogbone tensile specimen 203 mm in length, approximately 15.5 mm in width at grip section and 10.3 mm in width at gage section

[b] Dogbone tensile specimen 152 mm in length, approximately 12.6 mm in width at grip section and 10.3 mm in width at gage section

[s] Straight-sided tensile specimen152 mm in length and approximately 12.6 mm in width throughout.

Table II: Tow Size and Shape for Representative Composites

Composite Specimen	Architecture, Fiber-type	# of tows measured	2a, mm	2b, mm
HN 8 PLY (BN1)	Standard 8 ply, HN	30	0.13±0.02	1.15±0.09
HN 8 PLY (BN2)	Standard 8 ply, HN	33	0.14±0.02	1.19±0.10
HN 8 PLY (BN3)	Standard 8 ply, HN	15	0.13±0.02	1.21±0.10
HN 8 PLY (C)	Standard 8 ply, HN	32	0.14±0.02	1.22±0.20
E8Ply-8HS(BN)	Epoxy infiltrated 8HS, HN	23	0.14±0.02	1.17±0.14
3 Ply (C)	Thin (3 Ply), HN	15	0.14±0.02	1.18±0.09
7.9 epcm Syl-iBN (BN1)	Balanced, Syl-iBN	32	0.11±0.02	1.04±0.10
7.9 epcm Syl-iBN (BN2)	Balanced, Syl-iBN	--	0.11*	1.015*
7.9 epcm Syl-iBN (BN3)	Balanced, Syl-iBN	36	0.11±0.01	0.99±0.10
7.9 epcm Syl-iBN (C)	Balanced, Syl-iBN	32	0.11±0.01	1.17±0.10
9.4 epcm Syl-iBN (BN)	Unbalanced, Syl-iBN	63	0.11±0.01	1.13±0.10
5.5 epcm Syl-iBN (BN)	Unbalanced, Syl-iBN	59	0.10±0.01	1.08±0.08

* Average of 7.9 epcm Syl-iBN (BN1) and (BN3) panels were used

Table III: Moduli Measurements and Predictions for High Density Composites

Composite Specimen	Measured E_c, GPa	Predicted $E_{90\text{-inner}}$, GPa	Predicted E_c, GPa
Hi-Nicalon Composites			
HN 8 PLY (BN1)	258	175	261
HN 8 PLY (BN1)	269	175	258
HN 8 PLY (BN2)	243	157	251
HN 8 PLY (BN2)	225	157	253
HN 8 PLY (BN3)	225	180	244
HN 8 PLY (C)	199	90	226
HN 8 PLY (C)	195	90	215
HN 30 Ply (C)	237	194	261
HN 36 Ply (C)	231	183	250
Sylramic-iBN Composites			
7.9 epcm Syl-iBN (BN1)	247	153	247
7.9 epcm Syl-iBN (BN2)	254	156	253
7.9 epcm Syl-iBN (BN3)	278	148	279
7.9 epcm Syl-iBN (C)	230	63	223
9.4 epcm Syl-iBN (BN)	289	154	293
9.4 epcm Syl-iBN (BN)	293	154	303
5.5 epcm Syl-iBN (BN)	260	139	258
5.5 epcm Syl-iBN (BN)	261	140	263

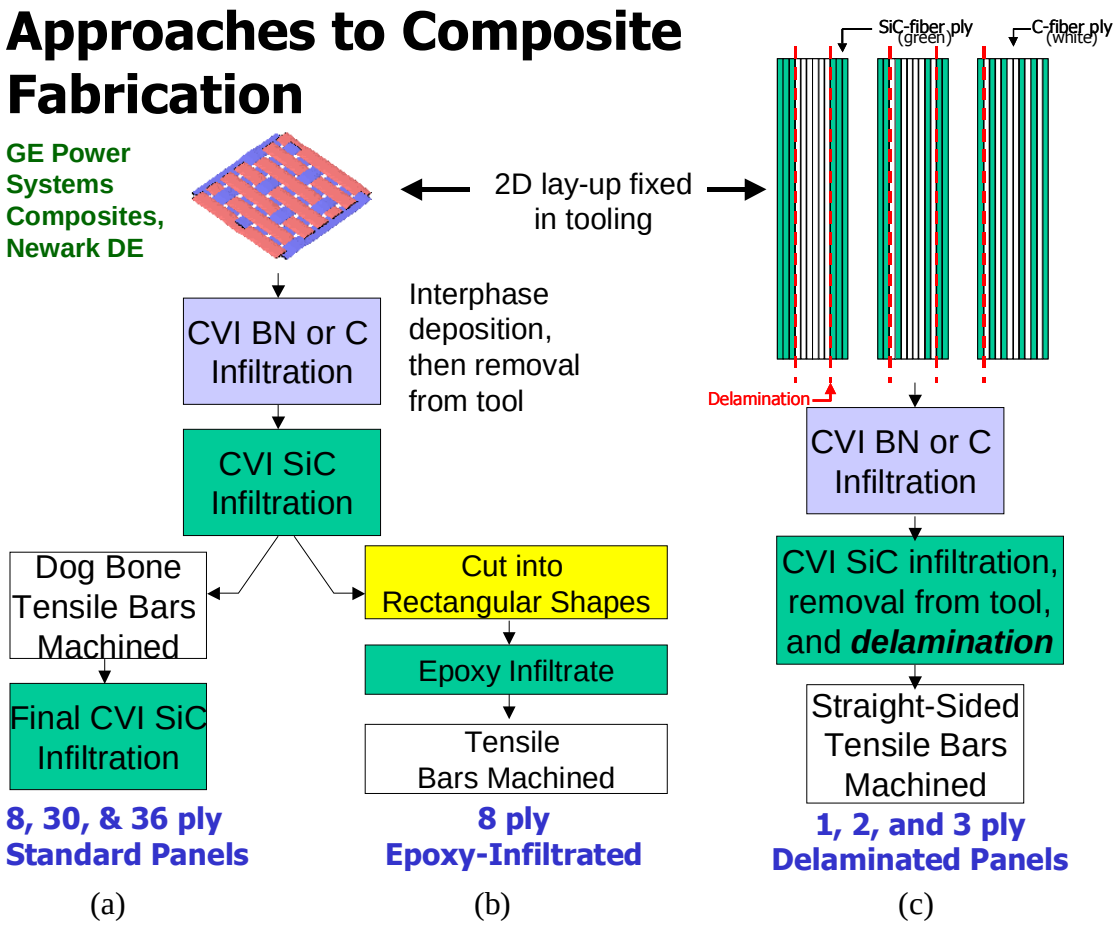

Figure 1: Approaches to composite fabrication

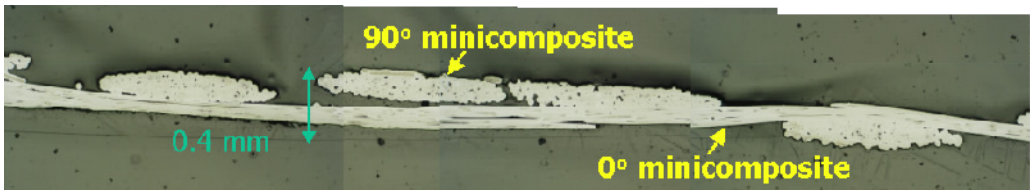

(a) HN 1 Ply Longitudinal Section

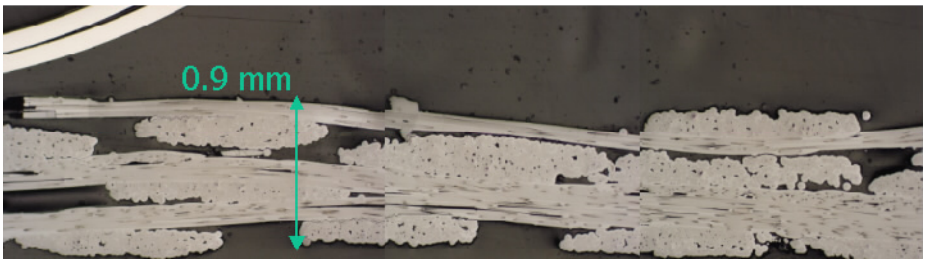

(b) HN 3 Ply Longitudinal Section

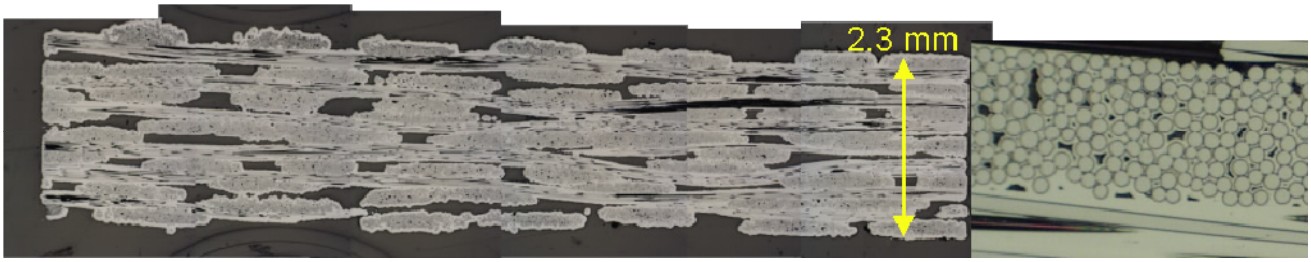

(c) HN 8 Ply (BN1) Cross-Section

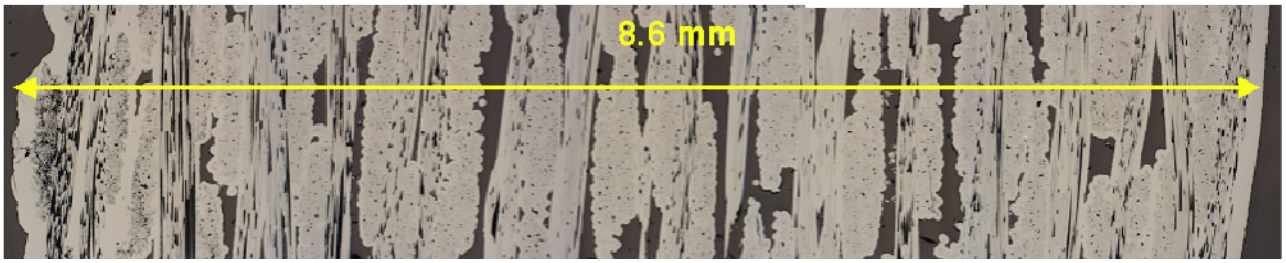

(d) HN 30 Ply Longitudinal Section

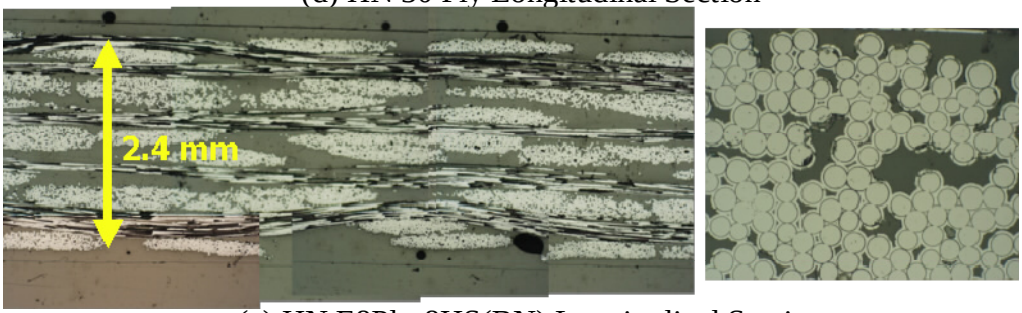

(e) HN E8Ply-8HS(BN) Longitudinal Section

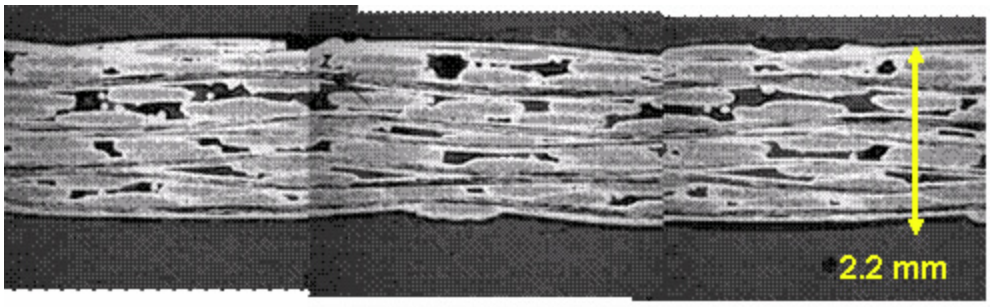

(f) Syl-iBN balanced 7.9 epcm

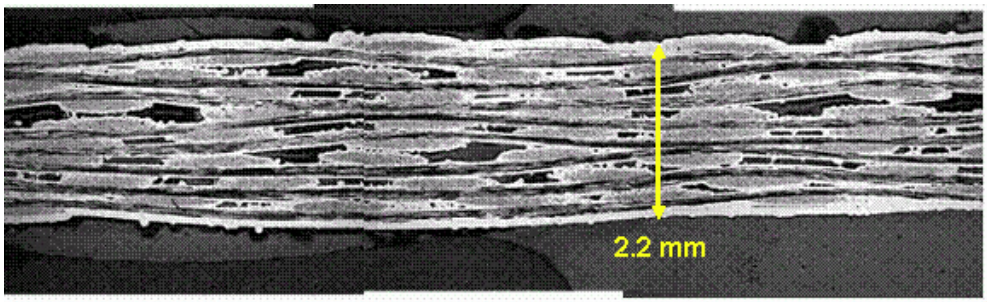

(g) Syl-iBN longitudinal (9.4 epcm) unbalanced

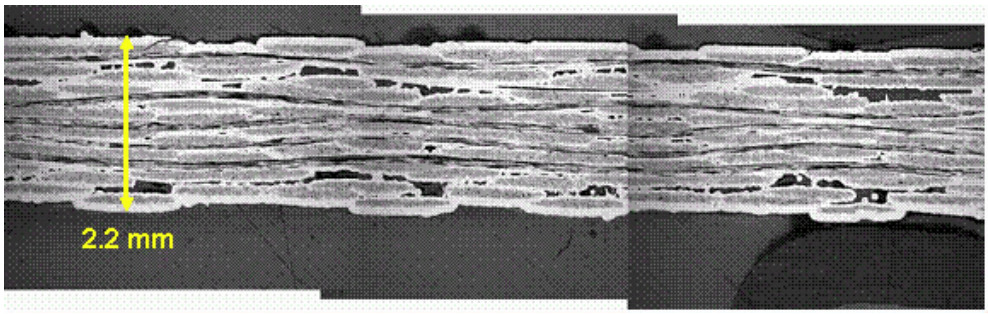

(h) Syl-iBN longitudinal (5.5 epcm) unbalanced

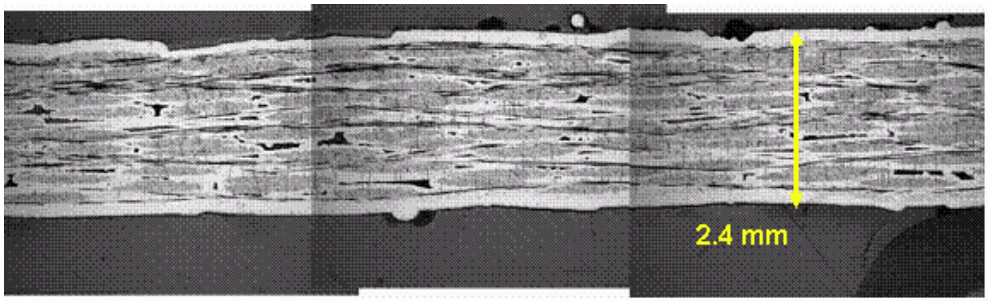

(i) Syl-iBN balanced 7.9 epcm with carbon interphase

Figure 2: Microstructures of selected CVI SiC matrix composites. All of the specimens have a BN interphase except for (i).

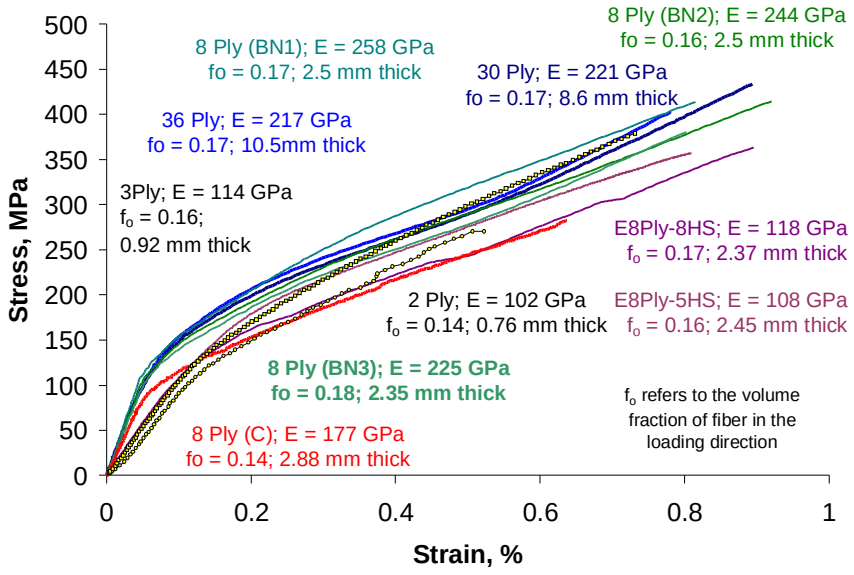

(a)

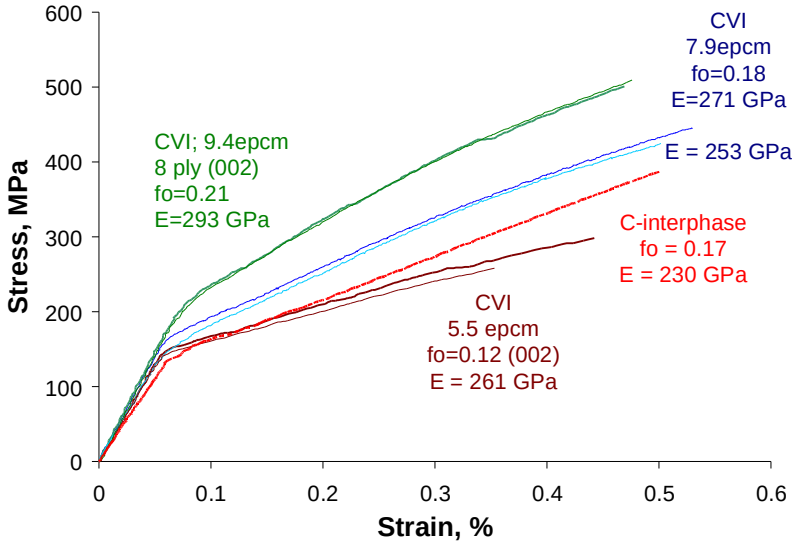

(b)

Figure 3: Tensile stress-strain behavior of (a) HN CVI SiC and (b) Syl-iBN CVI SiC composites.

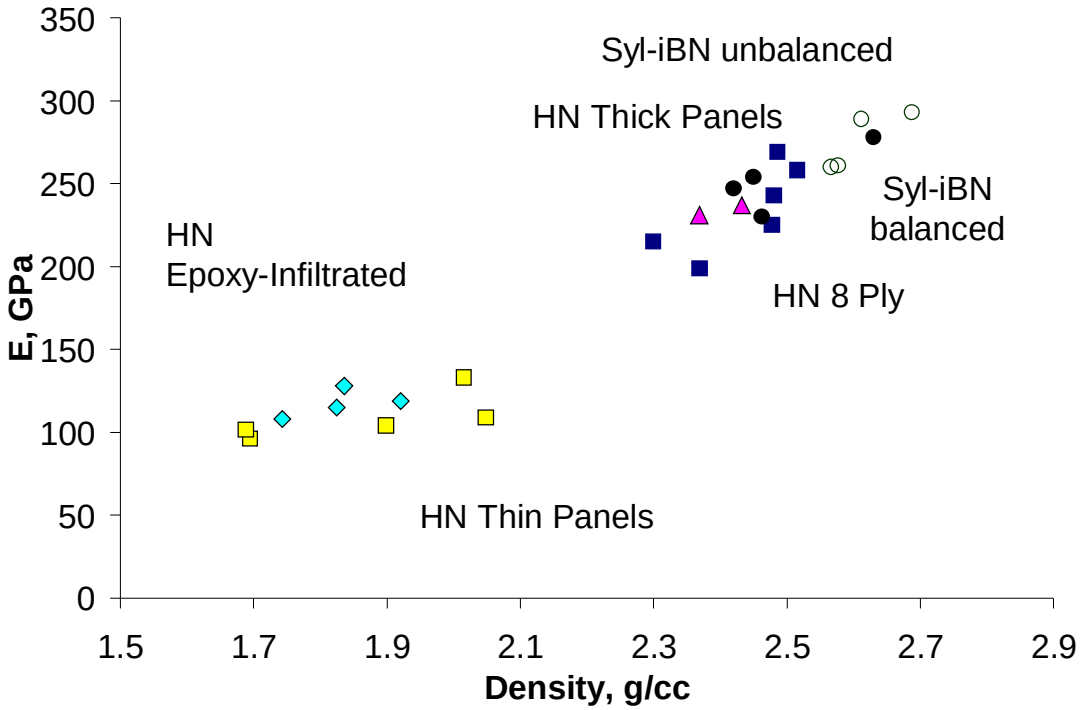

Figure 4: Effect of various physical properties on elastic modulus.

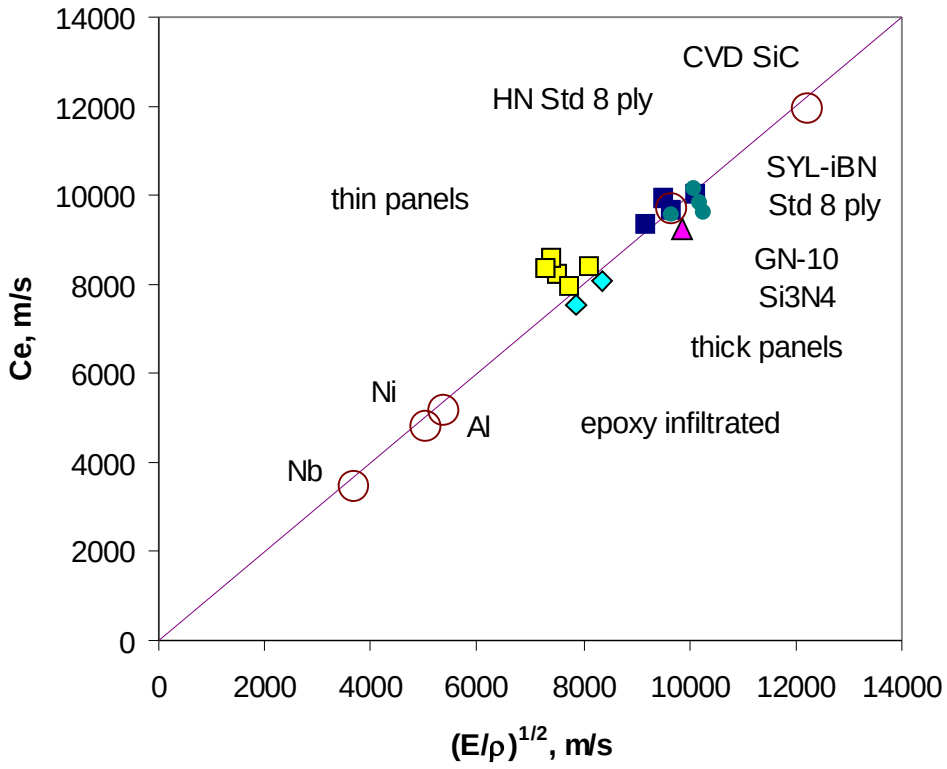

Figure 5: Measured speed of sound versus measured $(E/\rho)^{1/2}$.

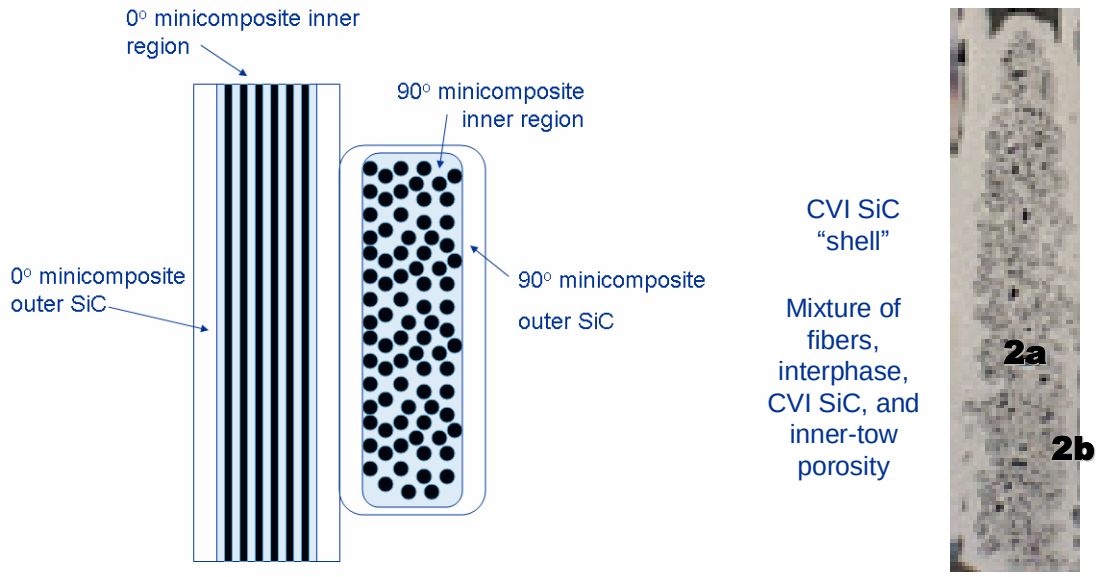

(a) (b)

Figure 6: Schematic representation (a) of 0^o and 90^o minicomposite construction and (b) a typical 90^o minicomposite from HN 8PLY (BN3).

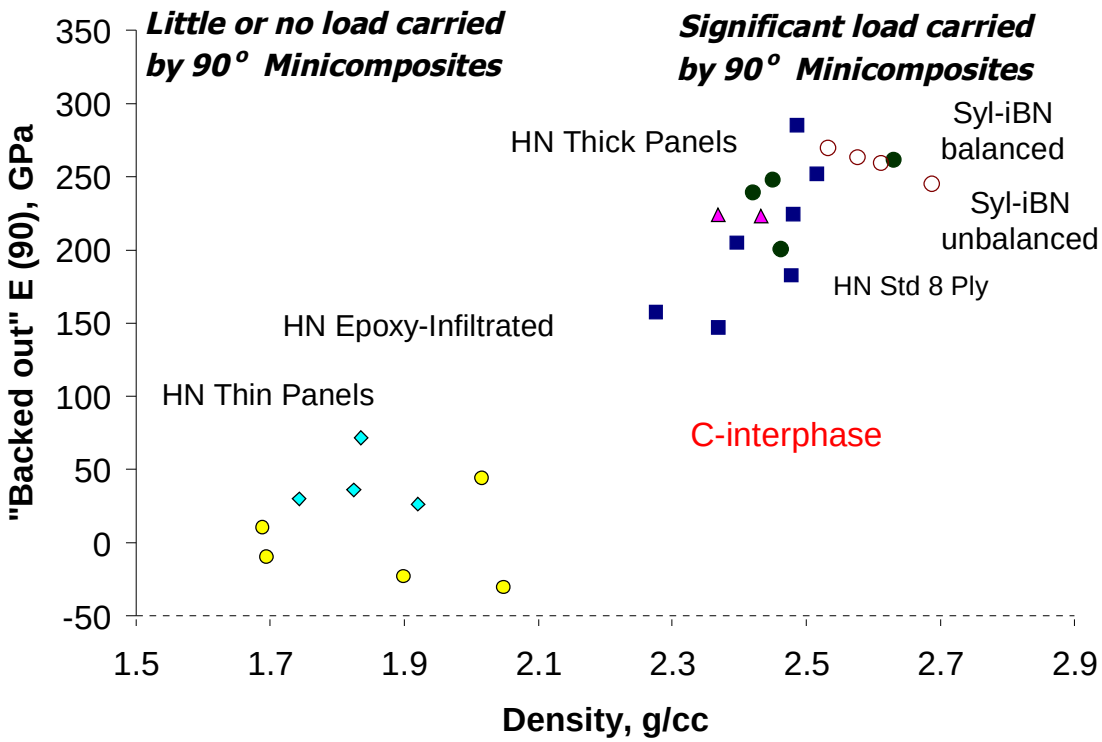

Figure 7: Effective elastic modulus of the 90° minicomposites.

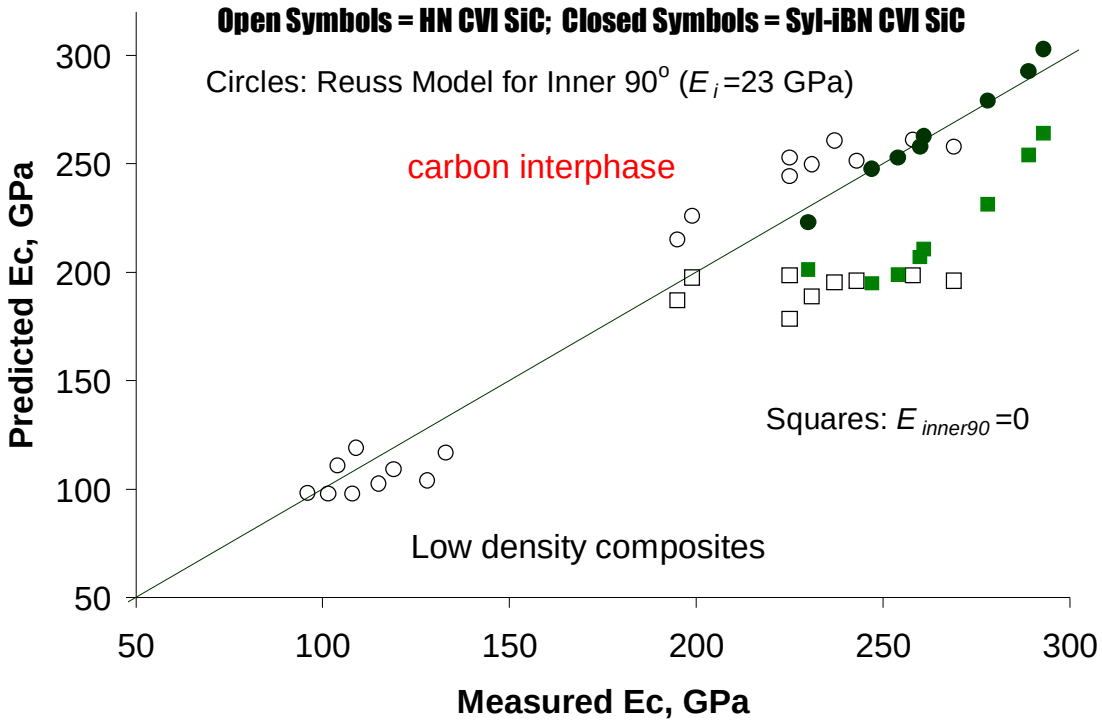

Figure 8: E_c prediction.